Inorganic Chemistry

Article

pubs.acs.org/IC

Facile Synthesis of Graphene/Metal Nanoparticle Composites via Self-Catalysis Reduction at Room Temperature

Qiqi Zhuo, Yanyun Ma, Jing Gao, Pingping Zhang, Yujian Xia, Yiming Tian, Xiuxiao Sun, Jun Zhong, and Xuhui Sun*

Institute of Functional Nano & Soft Materials (FUNSOM) and Jiangsu Key Laboratory for Carbon Based Materials and Devices, Soochow University, Suzhou, Jiangsu 215123, People's Republic of China

Supporting Information

ABSTRACT: Graphene/metal nanoparticle (NP) composites have attracted great interest for various applications as catalysts, electrodes, sensors, etc., due to their unique structures and extraordinary properties. A facile synthesis of graphene/metal NP composites with good control of size and morphology of metal NPs is critical to the practical applications. A simple method to synthesize graphene/metal NPs under a controllable manner via a self-catalysis reduction at room temperature has been developed in this paper. At first, metal NPs with desirable size and morphology were decorated on GO and then used as catalyst to accelerate the hydrolysis reaction of $NaBH_4$ to reduce the graphene oxide. Compared to the existing methods, the method reported here features several advantages in which graphene/metal NPs are prepared without using toxic and explosive reductant, such as hydrazine or its derivatives, making it environmentally benign, and the reaction can be processed at room temperature with high efficiency and in a large range of pH values. The approach has been demonstrated to successfully synthesize graphene composites with various metal NPs in large quantity, which opens up a novel and simple way to prepare large-scale graphene/metal or graphene/metal oxide composites under mild conditions for practical applications. For example, graphene/AuNP composites synthesized by the method show excellent catalytic capability.

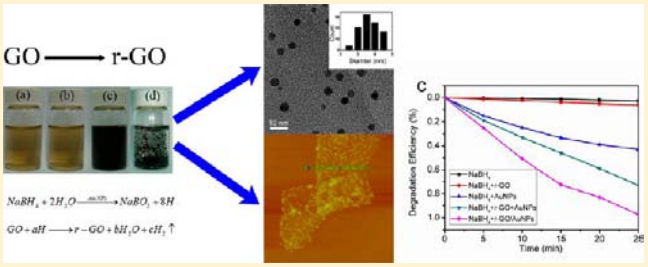

INTRODUCTION

Graphene-based composite materials have attracted enormous attention due to their unique structures and extraordinary properties for various applications as electrocatalysts,[1,2] electrodes,[3,4] sensors,[5] etc. Specifically, dispersion of metal NPs on graphene sheets potentially provides a novel way to develop catalysts, electrode materials, and so on.[6,7] A facile synthesis of graphene/metal NP composites with good control of size and morphology is critical to the practical applications. In general, there are two chemical methods to prepare graphene/metal NP composites. In a one-step method, metal precursor and graphene oxide (GO) sheets were mixed in aqueous solution and then reduced simultaneously to obtain the graphene/metal NP composite.[8,9] This method is easy and highly efficient. However, the size and morphology of metal NPs are hard to control during the reduction process, which can affect the function of the composite. The other one is a two-step method. At first, graphene (also called reduced graphene oxide, r-GO) and metal NPs were prepared by reducing GO and metal precursors, and then the r-GO/metal NP composite was obtained by mixing metal NPs with r-GO.[10−12] Compared to the one-step method, the morphology and size distribution of metal NPs can be exactly controlled in the two-step method. However, r-GO sheets are easily aggregated in most solutions after the reduction from GO due to the loss of the functional groups on the surface, and it is difficult to load metal NPs on the r-GO sheets uniformly with a high density.

A number of chemical reductants have been developed to reduce GO to form graphene/metal NP composites. For example, it has been reported that hydrazine or its derivatives could be used as the reductant to prepare graphene/metal NP composites.[13−15] However, these reductants are highly toxic and explosive, which limits their usage. In addition, other reductants can also be used for the synthesis of graphene/metal NP composites, such as benzylamine,[10] Na_2S,[8] and ethylene glycol.[9] However, most of above reactions were conducted at a high temperature beyond 80 °C,[8−10] which may introduce many defects in the graphene. Sodium borohydride ($NaBH_4$) is a thermally stable chemical hydride that has been extensively investigated as a potential hydrogen storage material and excellent reducing agent.[16] A number of metals have been demonstrated to be catalytically active toward the hydrolysis reaction of $NaBH_4$, such as Ni, Co, Pt, Pd, and Au.[17] These metal catalysts can greatly accelerate the hydrolysis reaction of $NaBH_4$ in ambient conditions. Although some research has been done on reducing GO by $NaBH_4$,[18,19] there has been little attention on catalyzing the hydrolysis reaction of $NaBH_4$ by metal to reduce GO at room temperature.

Received: November 28, 2012
Published: March 1, 2013

   dx.doi.org/10.1021/ic302608g | Inorg. Chem. 2013, 52, 3141−3147

Here, we developed a simple method to synthesize r-GO/metal NPs via a self-catalysis reduction at room temperature. This new two-step procedure represents a new way to prepare graphene/metal NP composites with several benefits: (i) The morphology and size of the metal NPs on graphene can be well controlled. (ii) Graphene is catalytically reduced after the deposition of the metal NPs on GO, leading to the uniform distribution of the NPs on graphene with high density. (iii) The graphene/metal NP composite is prepared without using toxic and/or explosive reductants, which is environmentally benign. (iv) The reaction proceeds at room temperature with high efficiency, resulting in the formation of fewer defects during the reduction process of GO. (v) The method can be applied in a large range of pH values. In addition, the simple and generic method may be applied for decorating r-GO sheets with most metal nanostructures and some metal oxide nanomaterials,[20,21] which perform the catalytic ability on the hydrolysis of $NaBH_4$.

EXPERIMENTAL SECTION

Chemicals. Graphite powder (~1000 mesh), H_2SO_4 (98%), $NaNO_3$, $KMnO_4$, H_2O_2 (30%), $HAuCl_4{\cdot}3H_2O$, and methylene blue (MB) were purchased from Sinopharm Chemical Reagent Co. Ltd. (Shanghai, China). Cetyltrimethylammonium bromide (CTAB), cetyltrimethylammonium chloride (CTAC), ascorbic acid (AA), and $NaBH_4$ were purchased from Alfa Aesar. Water used throughout all experiments was purified with the Millipore system.

Synthesis of GO. Graphene oxide (GO) was synthesized from graphite powder by a modified Hummers method.[22] In brief, graphite (1 g), $NaNO_3$ (0.5 g), and H_2SO_4 (25 mL) were added into a 250 mL beaker at 0 °C. Then, $KMnO_4$ (6 g) was added slowly into the beaker with stirring. After the temperature of the mixture was heated to 35 °C for 30 min, the solution was further heated to 90 °C and then 90 mL of water was slowly added under vigorous stirring for 15 min. Then, 60 mL of H_2O_2 aqueous solution was added to reduce the residual MnO_2. Finally, the yellow graphite oxides were washed by diluted HCl (3%) and water three times.

Synthesis of AuNPs. First, 5 mL of $HAuCl_4$ (0.5 M) and 5 mL of CTAB (0.2 M) were added into a 20 mL vial with stirring for 5 min. Then, 0.6 mL of 0.01 M $NaBH_4$ was added to the solution. After 2 h, 3 (±0.5) nm Au seeds were obtained. The chemisorbed Br^- in CTAB can prevent the aggregation of Au seeds to large Au nanocrystals.[23,24] The AuNPs with two larger sizes (9 and 25 nm) can be synthesized with the following process. Six milliliters of $HAuCl_4$ (0.5 M) and 6 mL of CTAC (0.02 M) were mixed into a 30 mL vial with stirring for 5 min, and then 4.5 mL of AA (0.1 M) was added to the solution. Finally, 0.3 and 0.01 mL of Au seeds of 3 (±0.5) nm was added to obtain AuNPs of 9 and 25 nm diameter, respectively.

Synthesis of GO/AuNPs and r-GO/AuNPs. One milliliter of as-prepared GO aqueous solution (1 mg/mL) was added into the 9 mL AuNP solution and sonicated for 5 min. The product of GO/AuNPs was collected by centrifugation and washed with DI water to remove the residual CTAB because excess CTAB may slow down the direct electron transfer of AuNPs, leading to reduced catalytic activity.[25] At room temperature, after 4 mg of $NaBH_4$ was added to 10 mL of GO/AuNP suspension (10 mM $NaBH_4$), the color was changed from brown to homogeneous black, indicating the reduction of GO/AuNPs. After 1 h, the r-GO/AuNP composite was separated by centrifugation and washed with DI water.

Reduction of MB. One milliliter of r-GO/AuNP (0.1 mg/mL) composite was added to 10 mL of MB solution (12 mg/L) with stirring for 1 h at 25 °C. Then, 1 mg of $NaBH_4$ was added to the solution. After reduction, the mixtures were centrifuged at 20 000 rpm for 5 min and the supernatant was put into a cuvette for a UV−vis spectroscopy test.

Characterization. The morphology of GO/AuNP and r-GO/AuNP sheets was characterized by transmission electron microscopy (TEM) (FEI Tecnai G2 F20 S-TIWN) with an accelerating voltage of 200 kV. The samples were applied to 300 mesh copper grids with lacey supported film. The thickness of the GO, GO/AuNP, and r-GO/AuNP sheets was measured by atomic force microscopy (AFM) (VeecoMultiMode V) under tapping mode. The scanning rate was 0.998 Hz, and the resonance vibration frequency was ~350 kHz. The samples for AFM measurement were prepared by dropping an aqueous suspension on the silicon chip. The surface state and electron structure of the composites were obtained by X-ray photoelectron spectroscopy (XPS) measurement (Kratos AXIS UltraDLD ultrahigh vacuum (UHV) surface analysis system), using Al Kα radiation (1486 eV) as a probe. The crystallographic structure of the materials was studied by a powder X-ray diffraction (XRD) (Empyrean, PANalytical B.V.) equipped with Cu Kα radiation (λ = 0.15406 nm). UV−vis detection was carried out on a LAMBDA 750 spectrometer (Perkin-Elmer). Fourier transform infrared (FTIR) spectra were recorded by a HYPERION 2000 spectrometer with ATR mode. Raman spectra were obtained on a Jobin-Yvon HR800 Raman spectrometer with 633 nm wavelength incident laser. The potential of GO, r-GO, and AuNPs were measured using a zeta-size analyzer (ZEN3690, Malvern).

RESULTS AND DISCUSSION

First, metal NPs were synthesized in a controlled manner as described in the Experimental Section and then added into as-prepared GO aqueous solution to form a light brown suspension of GO/metal NPs. $NaBH_4$ was added in the suspension to reduce GO at room temperature. After the reduction process, r-GO/metal NPs were collected by centrifugation and washed by DI water several times. By this method, AuNPs with different sizes, such as 3.5, 9, or 25 nm, were decorated on r-GO surfaces. Figure 1a shows the AFM image of an as-prepared GO sheet. The thickness of a single GO sheet is about 2 nm, which matches the results reported in the previous references.[26,27] Figure 1b shows the AFM image of a GO sheet decorated with 3.5 nm AuNPs. It is observed that a number of AuNPs are dispersed well on the surface of the GO sheet, and the thickness of GO/AuNP sheet is about 5.5 nm. The average diameter of AuNPs is around 3.5 nm. The morphology and structure of GO/AuNP sheets were characterized by TEM, as shown in Figure 1c,d. A TEM image with low magnification shows that the small AuNPs with narrow size distribution are uniformly distributed on the surface of GO sheets (Figure 1c). The average size of the AuNPs is about 3.5 nm as calculated by counting 100 AuNPs, consistent with the AFM result. The fringes with lattice spacing of 0.24 nm can be indexed as the planes of face-centered cubic (fcc) Au, as shown in the high-resolution TEM image in the inset of Figure 1d.

After the addition of $NaBH_4$, the brown color of the GO/AuNP solution (inset of Figure 2a) changed to black in 30 min, as shown in the inset of Figure 2c. After the reduction of GO for 60 min, the r-GO/AuNP sheets partially aggregated with each other (inset of Figure 2d). However, in a control experiment, there was no change in color even after adding $NaBH_4$ for 120 min without AuNPs (inset of Figure 2b). The reduction progress can be further monitored by UV−vis spectroscopy, as shown in Figure 2. The UV−vis absorption peak of GO/AuNP suspension at 228 nm (curve a) gradually shifts to 257 nm (curve c) and 262 nm (curve d) with the increase of reduction time, demonstrating that GO was reduced to graphene and the aromatic structure might be restored gradually.[28] Compared with the GO/AuNPs, the reduction rate of GO without AuNPs was much slower. Curve b in Figure 2 shows that the 228 nm peak has no change even when the reaction time was extended to 120 min. This result reveals that AuNPs can act as the catalyst to greatly accelerate the

dx.doi.org/10.1021/ic302608g | Inorg. Chem. 2013, 52, 3141−3147

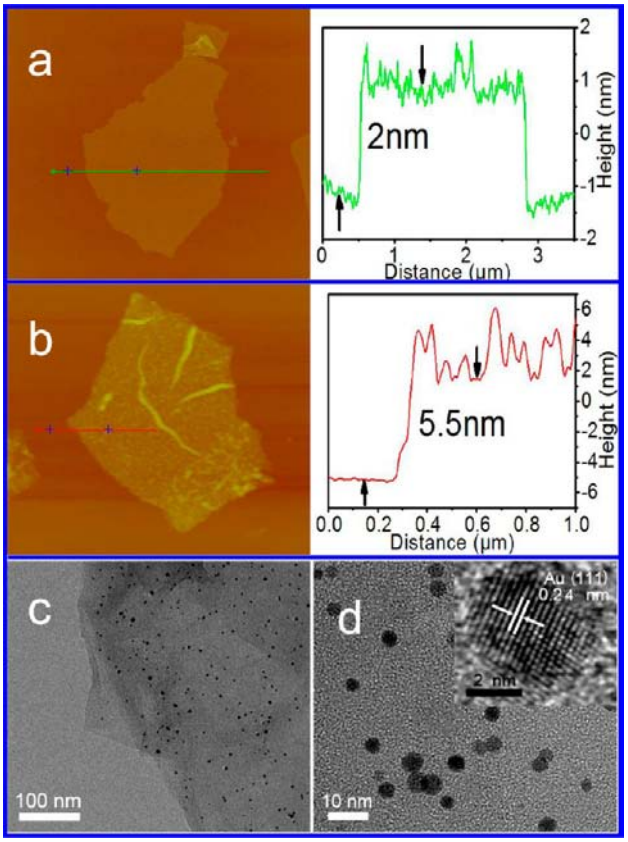

Figure 1. AFM images of a single GO sheet (a) and a GO sheet decorated with 3.5 nm AuNPs (b). The corresponding curves on the right side show the thicknesses of the GO sheet and the GO/AuNP sheet. (c,d) TEM images of the GO/AuNP sheet with different magnifications. Inset of (d) is the high-resolution TEM image of a single AuNP.

hydrolysis reaction of $NaBH_4$. The catalytic mechanism of metal on the hydrolysis of $NaBH_4$ had been studied previously and can be expressed as follows:[29,30]

$$2M + BH_4^- \rightleftharpoons H-\underset{\displaystyle M}{\overset{\displaystyle H}{\underset{|}{\overset{|}{B^-}}}}-H + M-H \quad (a)$$

$$H-\underset{\displaystyle M}{\overset{\displaystyle H}{\underset{|}{\overset{|}{B^-}}}}-H \rightleftharpoons BH_3 + M + e^- \quad (b)$$

$$BH_3 + OH^- \rightarrow BH_3OH^- \quad (c)$$

$$BH_3OH^- + 3OH^- \rightarrow BO_2^- + 3H + 2H_2O + 3e^- \quad (d)$$

$$4M + 4e^- + 4H_2O \rightarrow 4M - H + 4OH^- \quad (e)$$

$$M - H + 4M - H \rightleftarrows 5M + 5H \quad (f)$$

where M represents a surface site on the catalyst.

Then the hydrogen atoms released during the hydrolysis can reduce the oxygenous groups on the GO according to the following equation.

$$GO + aH \rightarrow \text{r-GO} + bH_2O + cH_2$$

After reduction, the AuNPs have no change on r-GO in composition and even morphology, which further proves the catalytic role of AuNPs.

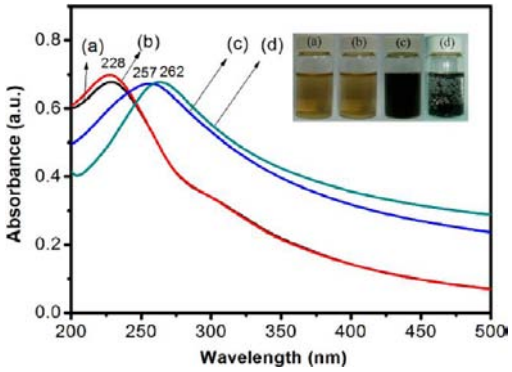

Figure 2. UV−vis absorption spectra of GO decorated with or without AuNPs. The reduction time of GO/AuNP sheets was 0 min (a), 30 min (c), and 60 min (d). (b) UV−vis spectrum of GO without AuNPs after being reduced for 120 min.

Figure 3a−d shows the AFM and TEM images of r-GO nanosheets with 3.5 nm AuNPs after the reduction of GO/AuNP sheets. Compared with GO/AuNP sheets, the morphology of r-GO/AuNP sheets does not show obvious change. The average size of AuNPs does not change and is still around 3.5 nm, shown in the histogram (inset of Figure 3d) by counting 100 AuNPs. The tight attachment of AuNPs on the sheet and the mild reduction condition prevent the change of the size and density of AuNPs in the GO reduction process. The size of AuNPs on the r-GO can be well controlled by the first step; for example, 9 and 25 nm AuNPs with small distribution on r-GO were obtained, shown in Figure 3e−h. TEM images with low magnification show that all AuNPs were attached on the r-GO sheet and no isolated AuNP outside the r-GO sheet was observed (see Supporting Information Figure S1). AuNPs were anchored on the r-GO sheet by electrostatic self-assembly. The zeta-potential test shows that the potentials of GO, rGO, and CTAC/CTAB-coated AuNPs are −45, −15, and +12 mV, respectively. Once the two oppositely charged materials, GO and AuNPs, are mixed, they are coupled to form a stable hybrid nanocomposite based on the electrostatic self-assembly. After the reduction, there is still an electrostatic force between rGO and AuNPs, which maintains the AuNPs on the rGO sheet. In addition, the different morphology of the Au nanostructure (e.g., nanorods; see Figure S2) can be decorated on graphene by the same procedure. The approach can be applied to obtain the different metal NP/graphene composites; for example, Pt-NP/graphene and Pd-NP/graphene (see Figure S3) have been synthesized by the approach, as well.

The reduction process can also be investigated by complementary spectroscopic experiments. Figure 4a shows the spectra of Fourier transform infrared spectroscopy of GO before and after reduction by $NaBH_4$ with AuNPs as the catalyst. Before the reduction, the vibration and deformation bands of the O−H groups on GO are at 3367 and 1363 cm^{-1}, respectively; the stretching vibration band of C═O is at 1722 cm^{-1}; the stretching vibration band of C═C is at 1620 cm^{-1}; and the stretching vibration bands of C−O in epoxy and alkoxy are at 1224 and 1045 cm^{-1}, respectively. It demonstrated that GO nanosheets have many oxygenous groups. After the reduction, the intensities of all FTIR peaks that correlated to

dx.doi.org/10.1021/ic302608g | Inorg. Chem. 2013, 52, 3141−3147

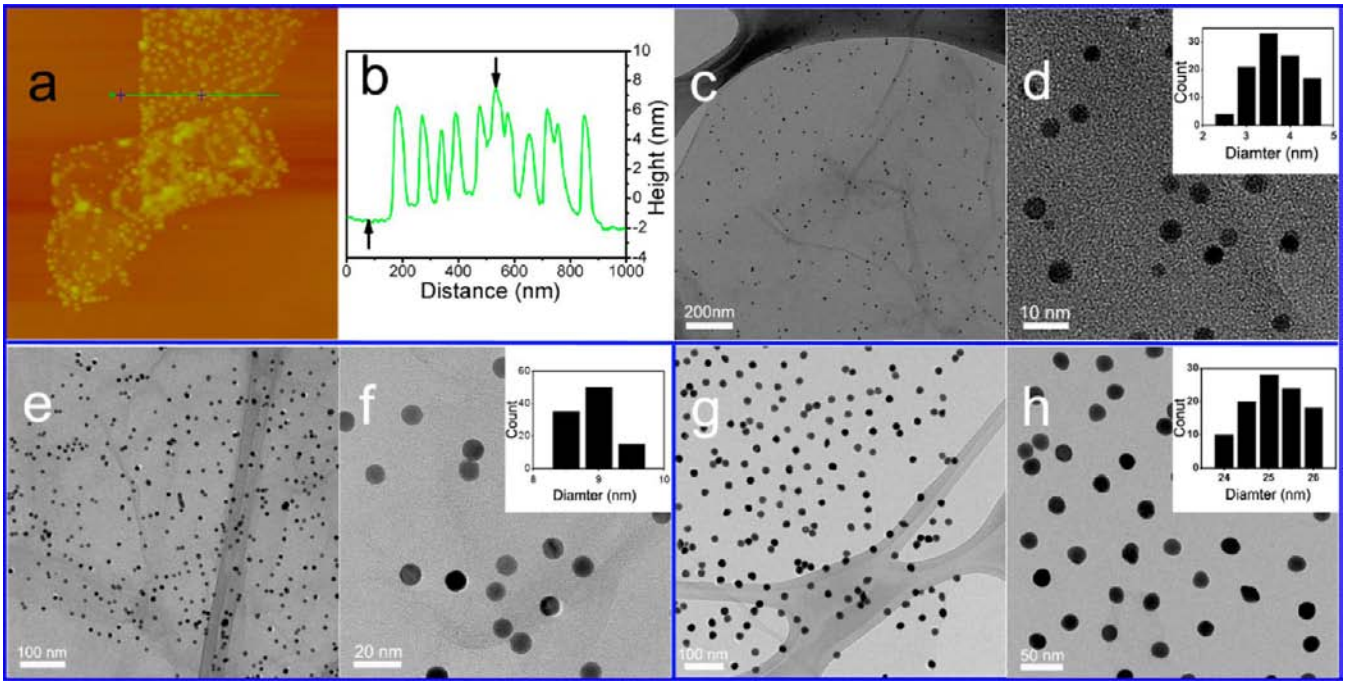

Figure 3. AFM image (a), height curve (b), and TEM images (c,d) of r-GO nanosheets with 3.5 nm AuNPs. TEM images of r-GO nanosheets with 9 nm (e,f) and 25 nm (g,h) AuNPs.

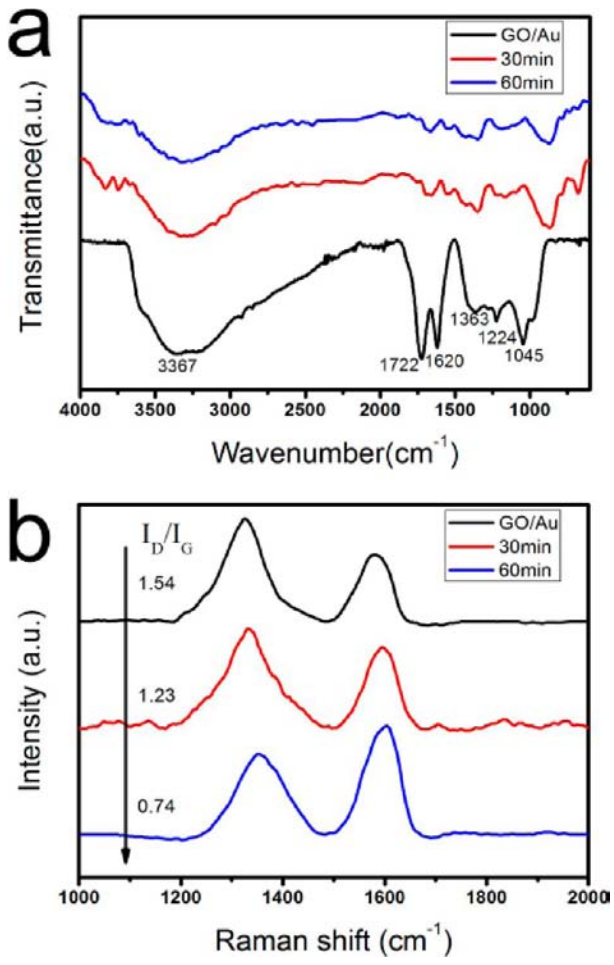

Figure 4. FTIR (a) and Raman (b) spectra of GO/Au and r-GO/Au with different reduction times (30 and 60 min).

the oxygenous groups decreased dramatically. Beyond that, Raman spectroscopy was used to evaluate the quality of r-GO because it is strongly sensitive to indicate single, conjugated, and double carbon−carbon bonds of carbon materials.[31] The G band at 1570−1600 cm^{-1} corresponds to the first-order scattering of the E_{2g} mode, and the D band at about 1350 cm^{-1} arises from a breathing mode of K-point phonons of A_{1g} symmetry.[32] As shown in Figure 4b, with the reduction progressing, the intensity ratio (I_D/I_G) gradually decreased from 1.54 to 1.23 after 30 min, and even to 0.74 after 60 min, indicating that the new domains of conjugated carbon atoms were formed after the removal of the oxygenous groups.

The reduction of oxygenous groups can be examined by X-ray photoelectron spectroscopy (XPS), as well. In Figure 5, with the increase of reduction time from 0 to 30 min and 60 min, the atomic ratio of carbon and oxygen (C/O) increased from 0.67 to 1.49 and finally 7.90, respectively. The intensities of all of the C1s peaks of the carbons bound to oxygen decreased gradually because most of the oxygenous functional groups were removed. Five different peaks centered at 284.6, 285.6, 286.8, 287.8, and 288.8 eV are observed, corresponding to sp^2-C, sp^3-C, −C−O, −C═O, and −COO− groups in the narrow areas of the C1s region, respectively. The C−O group is the most abundant among the oxygenous groups followed by C═O and COO− (Figure 5a). With the increase of reaction time, the peak of sp^3-C also decreased obviously; on the contrary, the peak of sp^2-C significantly increased, indicating that the reduction process is attributed to the restoration of the sp^2-C network.[32] In the meantime, the amount of C−O bonds decreased greatly and carbonyl groups decreased slightly, and there was no obvious change in the amount of carboxyl groups (Figure 5b) after 30 min. Then all of the oxygenous groups were removed after 1 h (Figure 5c). Previous research[19] found carbonyl groups on graphene were first transformed into C−O bonds at relatively low $NaBH_4$ content (15 mM), and carboxyl groups were partially removed. With the increase of $NaBH_4$ to

dx.doi.org/10.1021/ic302608g | Inorg. Chem. 2013, 52, 3141−3147

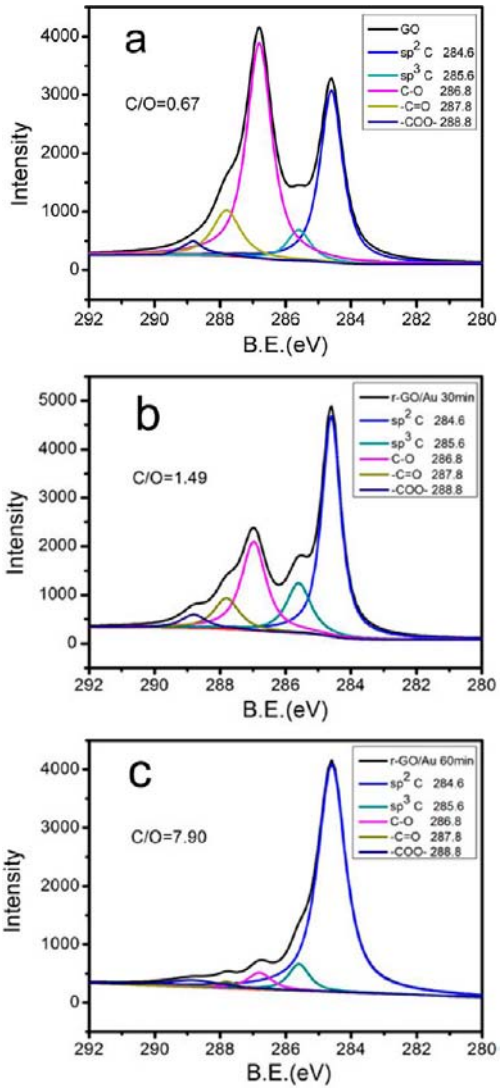

Figure 5. XPS C1s spectra of GO/Au and r-GO/Au at different reduction times: (a) 0 min, (b) 30 min, and (c) 60 min.

50 mM, all of the carbonyl groups were nearly removed, and the C−O bonds were reduced, as well. No significant reduction of the oxygen-related functional groups was observed at the higher $NaBH_4$ concentration of 150 mM. Some amount of oxygen atoms was retained in the film even after treatments involving high molarity.[19] In our study, although 10 mM $NaBH_4$ was used in the reduction, C−O bonds were greatly reduced at the beginning. We attribute it to the more active reduction capability of the hydrogen atoms released from the catalytic decomposition of $NaBH_4$ by AuNPs. It is one of the merits of this method that $NaBH_4$ can reduce GO at room temperature with high efficiency. It needs further investigation whether AuNPs have a synergic catalysis effect on the reduction of GO except for the catalytic hydrolysis reaction of $NaBH_4$.

In addition, the crystal structures of GO/AuNP and r-GO/AuNP composites were characterized by XRD, as shown in Supporting Information Figure S4. After reduction for 60 min, the peak of GO at 12.0° disappeared completely, resulting from the significant reduction of GO.[33]

It has been known that pH value is an important factor that effects the reduction of GO.[34,35] The hydrolysis reaction rate of $NaBH_4$ can be expressed by its half-life $t_{1/2}$ as the time requested to hydrolyze 50% of $NaBH_4$, which is as a function of pH value and temperature T (K):[17]

$$\log(t_{1/2}) = \mathrm{pH} - (0.034T - 1.92)$$

According to the equation, the smaller the pH value, the faster the reduction. Figure 6a shows the absorption peak

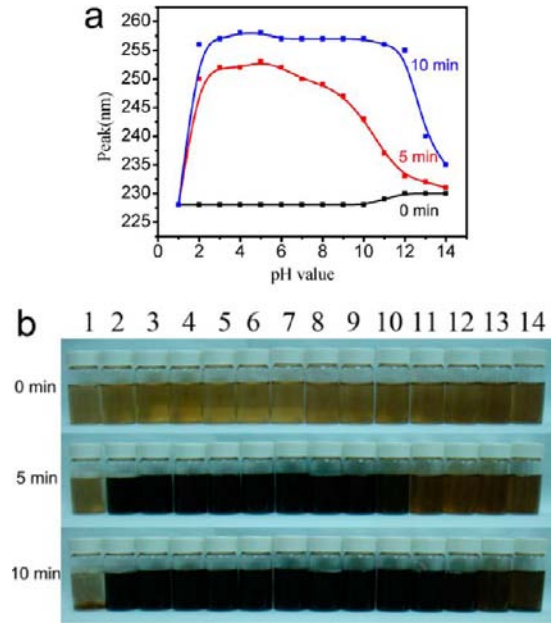

Figure 6. Absorption peaks in UV−vis spectra (a) and the corresponding photos (b) of the products when GO/AuNPs were reduced to r-GO/AuNPs at different pH values (1−14) with different times: 0, 5, and 10 min.

position of GO in UV−vis spectroscopy when GO/AuNPs were reduced to r-GO/AuNPs at different pH values with different times. As we discussed above, the shift of the absorption peak position toward high wavelength represents the reduction content of GO. It can be seen that the rate of the reduction in acidic conditions was much faster than that in alkaline conditions because the hydrolysis reaction rate of $NaBH_4$ in acidic conditions is much faster than in alkaline conditions. However, GO can also be reduced to rGO in alkaline conditions when the reduction time increased to 10 min (Figure 6a), which demonstrates that GO/AuNPs still show high catalytic capability for the hydrolysis reaction of $NaBH_4$ in alkaline conditions. It has been proven that the reduction of GO can occur in a large range of pH values. These phenomena could also be observed directly in their corresponding photos (Figure 6b). After the reduction, the light brown of GO changed to the dark r-GO.

In order to evaluate the catalytic capability of r-GO/AuNPs, the reduction of MB solution by $NaBH_4$ with different catalysts was carried out. Due to the high surface area of graphene (r-GO), it can highly absorb dye in solution.[36−38] One hour of stirring was needed to ensure the adsorption equilibrium between r-GO and MB so that the absorption effect can be eliminated. Figure 7a shows UV−vis adsorption spectra of MB that was mixed with r-GO and r-GO/Au and stirred for 1 h. It shows that around 12% MB was absorbed by r-GO or r-GO/Au. Figure 7b shows the UV−vis absorption spectra of an aqueous solution of MB in the presence of r-GO/AuNPs and $NaBH_4$ at different reaction times. The density of the peak at

dx.doi.org/10.1021/ic302608g | Inorg. Chem. 2013, 52, 3141−3147

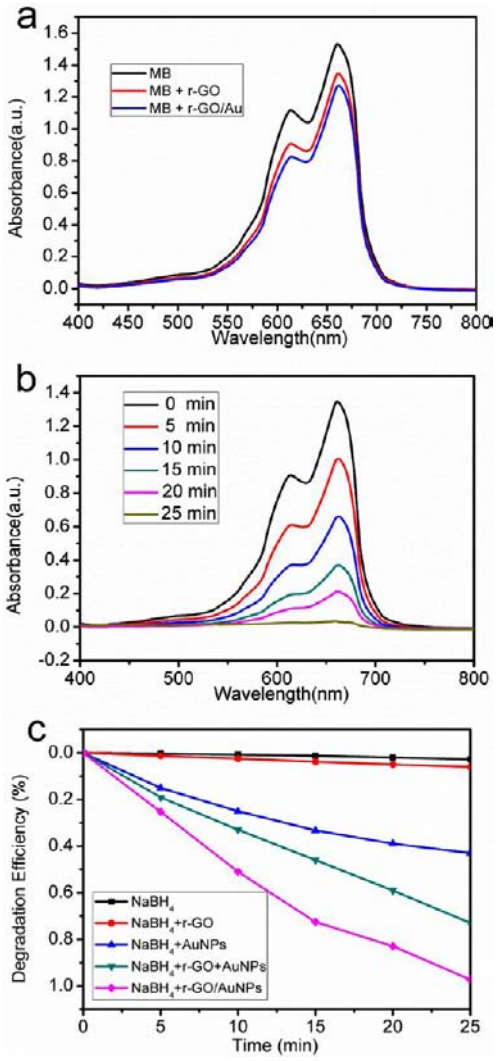

Figure 7. UV−vis absorption spectra of MB after mixed with r-GO and r-GO/Au (a), UV−vis absorption spectra of MB degradation by r-GO/AuNPs with different time (b), time profiles of MB degradation over $NaBH_4$, $NaBH_4$/r-GO, $NaBH_4$/AuNPs, $NaBH_4$ with the physical mixture of AuNPs and r-GO, and $NaBH_4$/r-GO/AuNPs (c).

665 nm gradually decreases with the increase of the reaction time, representing the degradation degree of MB. More than 12% MB was reduced within 5 min after $NaBH_4$ was added in the solution, which confirms that the decrease of the intensity of MB is mainly due to the reduction of MB under the r-GO/AuNP catalysis rather than the adsorption of r-GO. The peak disappears after 25 min, which suggests complete degradation of MB. By monitoring the MB absorption peak at 665 nm, we obtained plots of the percentage degree of degradation versus reaction time for different catalysts such as r-GO, AuNPs, the physical mixture of r-GO and AuNPs, and r-GO/AuNP composites (Figure 7c). The percentage degree of degradation was calculated by using $(C_0 - C) \times 100/C_0$, where C_0 is the initial concentration of MB, and C is the concentration of MB after degradation. The degradation was very slow using $NaBH_4$ and $NaBH_4$/r-GO without AuNP catalyst, and the degradation degree only reached 2.8 and 6% in 25 min, respectively. When r-GO/AuNPs were added into MB as the catalyst, MB was completely degraded in 25 min. It is demonstrated that r-GO/AuNPs can greatly accelerate the hydrolysis reaction of $NaBH_4$ to degrade MB. Compared to r-GO/AuNPs sheets, AuNPs without r-GO sheets and the physical mixture of r-GO and AuNPs also can accelerate the reduction, but their reduction rates are much slower than that of r-GO/AuNPs. AuNPs without r-GO as a carrier may easily aggregate together after adding into the MB solution, which decreases the catalytic capability. In addition, the absorption of MB on r-GO via $\pi-\pi$ stacking interactions, as MB is π-rich in nature,[38] provides a high local concentration of MB near the AuNPs, leading to highly efficient contact between them for the catalytic reduction.

CONCLUSIONS

In summary, we demonstrate a generic and mild method to synthesize r-GO/noble metal NP composites with well-controlled morphology and size. TEM and AFM images show that metal NPs with narrow size distribution are uniformly dispersed on the surface of graphene sheets. All of the results from UV−vis absorption spectroscopy, FTIR, Raman, XRD, and XPS consistently confirmed that most oxygenous groups were removed and the sp^2-C network was restored during the reduction process. The key merit of this method is the absence of toxic and/or explosive reductants, making the reaction environmentally benign. In addition, the reaction can be carried out at room temperature which introduces fewer defects during the reduction process and in a large range of pH values. This simple approach opens up a new way to prepare graphene/metal NP composites in large-scale under a mild condition. The graphene/metal NP composite shows excellent performance in catalyst applications.

ASSOCIATED CONTENT

Supporting Information

TEM images of r-GO/AuNPs, r-GO/PtNPs, and r-GO/PdNPs with different magnifications; TEM images of r-GO/Au nanorods and HRTEM images of Au nanorods; XRD patterns of the graphite, GO/AuNPs and r-GO/AuNPs. This material is available free of charge via the Internet at http://pubs.acs.org.

AUTHOR INFORMATION

Corresponding Author

*Phone: +86-512-65880943. Fax: +86-512-65882846. E-mail: xhsun@suda.edu.cn.

Notes

The authors declare no competing financial interest.

ACKNOWLEDGMENTS

This work was supported by the National Basic Research Program of China (973 Program) (Grant No. 2010CB934500), Natural Science Foundation of China (NSFC) (Grant No. 51072127), the Priority Academic Program Development of Jiangsu Higher Education Institutions.

REFERENCES

(1) Xiao, F.; Song, J.; Gao, H.; Zan, X.; Xu, R.; Duan, H. *ACS Nano* **2012**, *6*, 100−110.

(2) Kou, R.; Shao, Y.; Mei, D.; Nie, Z.; Wang, D.; Wang, C.; Viswanathan, V. V.; Park, S.; Aksay, I. A.; Lin, Y.; Wang, Y.; Liu, J. *J. Am. Chem. Soc.* **2011**, *133*, 2541−2547.

(3) Park, H.; Brown, P. R.; Bulovic, V.; Kong, J. *Nano Lett.* **2012**, *12*, 133−140.

(4) Zheng, Q.; Ip, W. H.; Lin, X.; Yousefi, N.; Yeung, K. K.; Li, Z.; Kim, J. K. *ACS Nano* **2011**, *5*, 6039−6051.

(5) Deng, S.; Tjoa, V.; Fan, H. M.; Tan, H. R.; Sayle, D. C.; Olivo, M.; Mhaisalkar, S.; Wei, J.; Sow, C. H. *J. Am. Chem. Soc.* **2012**, *134*, 4905−4917.
(6) Xiang, G.; He, J.; Li, T.; Zhuang, J.; Wang, X. *Nanoscale* **2011**, *3*, 3737−3742.
(7) Matyba, P.; Yamaguchi, H.; Chhowalla, M.; Robinson, N. D.; Edman, L. *ACS Nano* **2011**, *5*, 574−580.
(8) Chen, S.; Zhu, J. W.; Wang, X. *J. Phys. Chem. C* **2010**, *114*, 11829−11834.
(9) Xu, C.; Wang, X.; Zhu, J. W. *J. Phys. Chem. C* **2008**, *112*, 19841−19845.
(10) Liu, S.; Tian, J. Q.; Wang, L.; Sun, X. P. *Carbon* **2011**, *49*, 3158−3164.
(11) Zhang, S.; Shao, Y.; Liao, H.-g.; Liu, J.; Aksay, I. A.; Yin, G.; Lin, Y. *Chem. Mater.* **2011**, *23*, 1079−1081.
(12) Li, H. Q.; Han, L. N.; Cooper-White, J. J.; Kim, I. *Nanoscale* **2012**, *4*, 1355−1361.
(13) Guo, S. J.; Dong, S. J.; Wang, E. W. *ACS Nano* **2010**, *4*, 547−555.
(14) Wang, S.; Wang, X.; Jiang, S. P. *Phys. Chem. Chem. Phys.* **2011**, *13*, 6883.
(15) Hu, Y.; Zhang, H.; Wu, P.; Zhang, H.; Zhou, B.; Cai, C. *Phys. Chem. Chem. Phys.* **2011**, *13*, 4083.
(16) Muir, S. S.; Yao, X. *Int. J. Hydrogen Energy* **2011**, *36*, 5983−5997.
(17) Chatenet, M.; Micoud, F.; Roche, I.; Chainet, E. *Electrochim. Acta* **2006**, *51*, 5459−5467.
(18) Li, J. F.; Lin, H.; Yang, Z. L.; Li, J. B. *Carbon* **2011**, *49*, 3024−3030.
(19) Shin, H. J.; Kim, K. K.; Benayad, A.; Yoon, S. M.; Park, H. K.; Jung, I. S.; Jin, M. H.; Jeong, H. K.; Kim, J. M.; Choi, J. Y.; Lee, Y. H. *Adv. Funct. Mater.* **2009**, *19*, 1987−1992.
(20) Hung, T. F.; Kuo, H. C.; Tsai, C. W.; Chen, H. M.; Liu, R. S.; Weng, B. J.; Lee, J. F. *J. Mater. Chem.* **2011**, *21*, 11754−11759.
(21) Simagina, V. I.; Komova, O. V.; Ozerova, A. M.; Netskina, O. V.; Odegova, G. V.; Kellerman, D. G.; Bulavchenko, O. A.; Ishchenko, A. V. *Appl. Catal. A* **2011**, *394*, 86−92.
(22) Hummers, W. S.; Offeman, R. E. *J. Am. Chem. Soc.* **1958**, *80*, 1339−1339.
(23) Bullen, C.; Zijlstra, P.; Bakker, E.; Gu, M.; Raston, C. *Cryst. Growth Des.* **2011**, *11*, 3375−3380.
(24) Xia, Y.; Xiong, Y.; Lim, B.; Skrabalak, S. E. *Angew. Chem., Int. Ed.* **2009**, *48*, 60−103.
(25) Gao, H.; Xiao, F.; Ching, C. B.; Duan, H. *ACS Appl. Mater. Interfaces* **2011**, *3*, 3049−3057.
(26) Park, S.; Ruoff, R. S. *Nat. Nanotechnol.* **2009**, *4*, 217−224.
(27) Nguyen, S. T.; Stankovich, S.; Dikin, D. A.; Piner, R. D.; Kohlhaas, K. A.; Kleinhammes, A.; Jia, Y.; Wu, Y.; Ruoff, R. S. *Carbon* **2007**, *45*, 1558−1565.
(28) Li, D.; Muller, M. B.; Gilje, S.; Kaner, R. B.; Wallace, G. G. *Nat. Nanotechnol.* **2008**, *3*, 101−105.
(29) Simoes, M.; Baranton, S.; Coutanceau, C. *J. Phys. Chem. C* **2009**, *113*, 13369−13376.
(30) Holbrook, K. A.; Twist, P. J. *J. Chem. Soc. (A)* **1971**, 890.
(31) Tien, H.-W.; Huang, Y.-L.; Yang, S.-Y.; Hsiao, S.-T.; Liao, W.-H.; Li, H.-M.; Wang, Y.-S.; Wang, J.-Y.; Ma, C.-C. M. *J. Mater. Chem.* **2012**, *22*, 2545−2552.
(32) Zhou, X. J.; Zhang, J. L.; Wu, H. X.; Yang, H. J.; Zhang, J. Y.; Guo, S. W. *J. Phys. Chem. C* **2011**, *115*, 11957−11961.
(33) Zhu, C.; Guo, S.; Fang, Y.; Dong, S. *ACS Nano* **2010**, *4*, 2429−2437.
(34) Li, D.; Müller, M. B.; Gilje, S.; Kaner, R. B.; Wallace, G. G. *Nat. Nanotechnol.* **2008**, *3*, 101−105.
(35) Fan, X. B.; Peng, W. C.; Li, Y.; Li, X. Y.; Wang, S. L.; Zhang, G. L.; Zhang, F. B. *Adv. Mater.* **2008**, *20*, 4490−4493.
(36) Zhang, Y. W.; Liu, S.; Lu, W. B.; Wang, L.; Tian, J. Q.; Sun, X. P. *Catal. Sci. Technol.* **2011**, *1*, 1142−1144.
(37) Qin, X. Y.; Lu, W. B.; Luo, Y. L.; Chang, G. H.; Asiri, A. M.; Al-Youbi, A. O.; Sun, X. P. *J. Nanosci. Nanotechnol.* **2012**, *12*, 2983−2989.
(38) Yang, S. T.; Chen, S.; Chang, Y. L.; Cao, A. N.; Liu, Y. F.; Wang, H. F. *J. Colloid Interface Sci.* **2011**, *359*, 24−29.